

ENVIRONMENTAL RESEARCH
LETTERS

LETTER

Climate drivers of Arctic tundra variability and change using an indicators framework

OPEN ACCESS

RECEIVED

29 December 2020

REVISED

7 February 2021

ACCEPTED FOR PUBLICATION

15 February 2021

PUBLISHED

6 May 2021

Original content from this work may be used under the terms of the [Creative Commons Attribution 4.0 licence](#).

Any further distribution of this work must maintain attribution to the author(s) and the title of the work, journal citation and DOI.



Uma S Bhatt^{1,9} , Donald A Walker², Martha K Reynolds², John E Walsh³, Peter A Bieniek³, Lei Cai⁴, Josefino C Comiso⁵ , Howard E Epstein⁶, Gerald V Frost⁷ , Robert Gersten⁵, Amy S Hendricks¹, Jorge E Pinzon⁸, Larry Stock⁵ and Compton J Tucker⁸

¹ Department of Atmospheric Sciences in the College of Natural Science and Mathematics, Geophysical Institute, University of Alaska Fairbanks, 903 Koyukuk Dr, Fairbanks, AK 99775-7320, United States of America

² Institute of Arctic Biology, University of Alaska Fairbanks, PO Box 757000, Fairbanks, AK 99775-7000, United States of America

³ International Arctic Research Center, University of Alaska, Fairbanks, PO Box 757340, Fairbanks, AK 99775-7340, United States of America

⁴ Department of Atmospheric Sciences, Yunnan University, North Cuihu Road 2, Kunming 650000, People's Republic of China

⁵ Cryospheric Sciences Branch, NASA, NASA Goddard Space Flight Center, Code 614.1, Greenbelt, MD 20771, United States of America

⁶ Department of Environmental Sciences, University of Virginia, 291 McCormick Rd., Charlottesville, VA 22904-4123, United States of America

⁷ ABR, Inc.—Environmental Research & Services, PO Box 80410, Fairbanks, AK 99708, United States of America

⁸ Biospheric Science Branch, NASA; NASA Goddard Space Flight Center, Code 614.1, Greenbelt, MD 20771, United States of America

⁹ Author to whom correspondence should be addressed.

E-mail: usbhatt@alaska.edu

Keywords: Arctic tundra, NDVI, sea-ice, Arctic Dipole, continentality, summer warmth index

Abstract

This study applies an indicators framework to investigate climate drivers of tundra vegetation trends and variability over the 1982–2019 period. Previously known indicators relevant for tundra productivity (summer warmth index (SWI), coastal spring sea-ice (SI) area, coastal summer open-water (OW)) and three additional indicators (continentality, summer precipitation, and the Arctic Dipole (AD): second mode of sea level pressure variability) are analyzed with maximum annual Normalized Difference Vegetation Index (MaxNDVI) and the sum of summer bi-weekly (time-integrated) NDVI (TI-NDVI) from the Advanced Very High Resolution Radiometer time-series. Climatological mean, trends, and correlations between variables are presented. Changes in SI continue to drive variations in the other indicators. As spring SI has decreased, summer OW, summer warmth, MaxNDVI, and TI-NDVI have increased. However, the initial very strong upward trends in previous studies for MaxNDVI and TI-NDVI are weakening and becoming spatially and temporally more variable as the ice retreats from the coastal areas. TI-NDVI has declined over the last decade particularly over High Arctic regions and southwest Alaska. The continentality index (CI) (maximum minus minimum monthly temperatures) is decreasing across the tundra, more so over North America than Eurasia. The relationship has weakened between SI and SWI and TI-NDVI, as the maritime influence of OW has increased along with total precipitation. The winter AD is correlated in Eurasia with spring SI, summer OW, MaxNDVI, TI-NDVI, the CI and total summer precipitation. This winter connection to tundra emphasizes the role of SI in driving the summer indicators. The winter (DJF) AD drives SI variations which in turn shape summer OW, the atmospheric SWI and NDVI anomalies. The winter and spring indicators represent potential predictors of tundra vegetation productivity a season or two in advance of the growing season.

1. Introduction

Indicators provide a framework for understanding complex ideas using simplified metrics that can be standardized, used for long-term monitoring, and communicated effectively with the broader public. The climate indicators framework was developed in order to support climate assessments (Kenny *et al* 2016) and was successfully implemented in the U.S. Global Climate Research Program (www.globalchange.gov, NASEM 2017). As researchers are challenged to understand the rapidly changing Earth system, the indicators framework is increasingly being used to monitor and document change. One such example is the NOAA Arctic Report Card (e.g. Richter-Menge *et al* 2019) that develops and updates essays annually on the atmosphere, ocean, sea-ice (SI), vegetation, and other indicator variables.

The indicators framework has been applied to understand Arctic climate change and variability. Box *et al* (2019) analyzed key Arctic indicators in physical (e.g. SI area, temperatures, precipitation) and biophysical (e.g. tundra productivity, disturbances, riverine biogeochemistry) systems jointly to document their linkages. Overland *et al* (2019) combined a set of Arctic indicators into a composite Arctic Climate Change Index as a way to document the manifestation of global change in the Arctic. In this study, we apply the indicators framework to climate drivers of Arctic tundra vegetation variability and trends, enabling a diagnosis of relevant drivers including several that can serve as seasonal-scale predictors of NDVI variations.

The Normalized Difference Vegetation Index (NDVI) is commonly used to monitor vegetation greenness (Tucker 1979, Frost *et al* 2020) and has been applied to Arctic tundra from the first analyses indicating enhanced greening at high latitudes (Myneni *et al* 1997, Jia *et al* 2003) and continuing through annual monitoring reports (e.g. NOAA State of the Climate and Arctic Report Card). NDVI contrasts surface reflectance in red (R) and near infrared (NIR) wavelengths (figure 1(a)), calculated as $(\text{NIR} - \text{R})/(\text{NIR} + \text{R})$. Most red light is absorbed by plants for photosynthesis, while NIR wavelengths are reflected by the complexities of the plant canopy. As vegetation cover increases particularly in less abundantly vegetated areas such as the Arctic, either spatially or temporally, additional red light is absorbed and more NIR radiation is reflected, increasing the NDVI (figure 1(a)). Over the summer, Arctic NDVI increases rapidly after snowmelt in late May to early June, peaks in July and August, and decreases slowly until the first snowfall (figure 1(b)).

The long-term satellite record indicates that 'greening' (increase in NDVI) is occurring in much of the Arctic tundra biome (non-glaciated land north of treeline), especially on Alaska's North Slope

(Jia *et al* 2003, Frost *et al* 2020). NDVI trends, however, vary spatially and temporally and have recently shown a general stabilization or even decline especially in Arctic North America. At circumpolar and continental scales, tundra vegetation and productivity vary considerably across north–south climate gradients, coastal–inland continentality gradients, and with east–west floristic differences (CAVM Team 2003, Raynolds *et al* 2019). At regional scales, geology, elevation, and physiography strongly affect vegetation patterns, and at landscape and plot scales, small differences in microrelief, soil moisture, and disturbance strongly affect vegetation patterns (Walker *et al* 2016). Field studies have documented the highly variable nature of the NDVI response to local temperature gradients, local precipitation, surface wetness, changes in the length of the snow-free period, growing season length, extreme weather events, and large disturbances such as fire, floods, and insect outbreaks (e.g. Trofaier *et al* 2013, Raynolds and Walker 2016, Bjerke *et al* 2017).

This study applies an indicator framework to explore trends and variability in Arctic NDVI relative to a few key parameters, some used in previous work and some new. The Advanced Very High Resolution Radiometer (AVHRR) maximum annual NDVI (MaxNDVI) and summed growing season bi-weekly (i.e. time-integrated) NDVI (TI-NDVI) time-series that now span from 1982 to 2019 form the core of this analysis, as they are the most direct observational indicators of tundra vegetation productivity for the full circumpolar Arctic using reasonably consistent sensor platforms with a long period of record. The other indicators that will be used in the study are chosen because of their established or hypothesized importance for NDVI. The amount of springtime SI in nearshore (100 km buffer) coastal waters influences the total summer open-water (OW) area and available summer warmth for vegetation productivity in the Arctic tundra, which is a maritime biome (Walker *et al* 2005). The decline in Arctic SI plays a key role in NDVI increases, since land surface temperatures become warmer once SI melts along the coast (Bhatt *et al* 2010, Dutrieux *et al* 2012). However, as the ice continues to decline, this relationship is weakening (Bhatt *et al* 2013) as other factors come into play. The total summer warmth depends on the timing of coastal SI melt and is described using the summer warmth index (SWI: sum of the degree months above freezing during April–September). Total summer precipitation (TSP) is a new indicator included in this context, because there is a growing body of evidence that the Arctic hydrological cycle is intensifying (Box *et al* 2019), will increase in the future (Bintanja and Selten 2014), and it influences tundra NDVI variations (Lara *et al* 2018, Campbell *et al* 2020). A continentality index (CI, the maximum minus minimum monthly temperature in a calendar

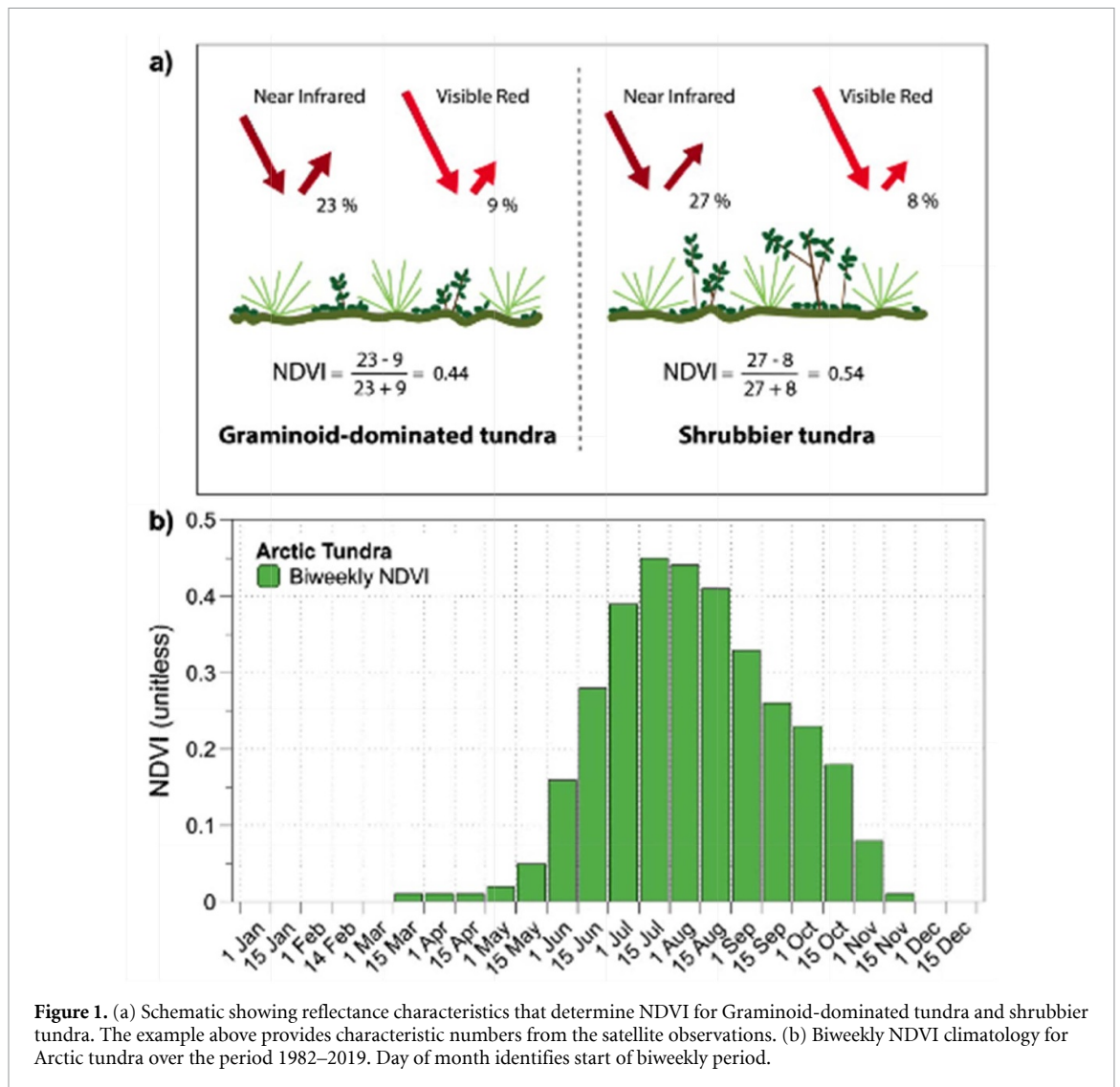


Figure 1. (a) Schematic showing reflectance characteristics that determine NDVI for Graminoid-dominated tundra and shrubbier tundra. The example above provides characteristic numbers from the satellite observations. (b) Biweekly NDVI climatology for Arctic tundra over the period 1982–2019. Day of month identifies start of biweekly period.

year) is introduced to provide a measure of atmospheric variability across seasons, since winter warming has also been found to impact vegetation productivity (Bokhorst *et al* 2009). Additional indicators that are introduced in the context of tundra variability are the first two modes of sea level pressure variability in the Arctic, the Arctic Oscillation (AO) (Thompson and Wallace 1998) and the Arctic Dipole (AD) (Wang and Ikeda 2000) (explained below).

This study presents the pan-Arctic and continental scale relationships between key indicators and tundra vegetation. We discuss each indicator variable through its climatology (long-term average) and spatial trends as shown in circumpolar maps, time-series graphs, and through the correlations between each of the variables and vegetation for Arctic, Eurasian, and North American Arctic tundra. Our goal is to identify the important parameters affecting tundra vegetation productivity and to better map the climate drivers operating on Arctic tundra vegetation. The sequencing of the processes across seasons will point to the potential for predicting NDVI at ranges of a season or two.

2. Data and methods

2.1. Data

Spatially distributed time series were calculated for ten environmental indicators for the 1982–2019 period: two measures of vegetation, two measures of SI, two temperature data sets, continentality, precipitation, and two teleconnection indices. Remotely-sensed 8 km resolution NASA GIMMS (Global Inventory Modeling and Monitoring System) bi-weekly composited maximum NDVI (MaxNDVI) data (Pinzon and Tucker 2014) from 1982 to 2019 were derived from AVHRR sensors on NOAA-7 through NOAA-19 satellites. The GIMMS NDVI3g V1.2 product corrected discontinuities in the GIMMS NDVI north of 72° N and permitted the first comprehensive analysis of NDVI trends in the High Arctic (Bhatt *et al* 2010). The GIMMS dataset used Sea-viewing Wide Field-of-view Sensor data for calibrating among the collection of used sensors (Pinzon and Tucker 2014). This study uses the 1/12° resolution NDVI data to more closely match the grids used for SI and surface temperature. The MaxNDVI

is the highest summer NDVI value, representing peak vegetation photosynthetic capacity, and serves as an indicator of peak tundra biomass (Tucker 1977, Myneni *et al* 1997). The TI-NDVI is the sum of biweekly values from May to September that exceed the threshold value of 0.05. TI-NDVI incorporates the length of the growing season and phenological variations, and represents net primary production better than MaxNDVI (Tucker and Sellers 1986).

Spring SI and OW were investigated using the Special Sensor Microwave Imager SI concentration data from 1982 to 2019 (Comiso and Nishio 2008). Spring SI concentration is the percentage of a pixel covered by ice during a 3 week averaged period centered on the week when that pixel has 50% climatological ice cover. The methodology to construct SI was chosen, because TI-NDVI is most strongly correlated with SI at 50% concentration (Bhatt *et al* 2010), and the timing of the 50% threshold varies across the Arctic. OW is the inverse, the portion of a pixel that was not covered by SI (i.e. 100%—SI concentration). Summer OW is the average of the weekly May through August OW percentage.

Both land surface and air temperatures were used to construct indicators in order to compare their variability and change. The AVHRR-derived land-surface-temperature data were corrected through effective cloud-masking techniques and calibrated using *in situ* surface-temperature data including temperatures from the Surface Heat Budget in the Arctic experiment conducted in the central Arctic from October 1997 through September 1998 and 2 m air temperatures from meteorological stations (Comiso *et al* 2003). The European Center Reanalysis version 5 (ERA5) (Hersbach *et al* 2020) was used for 2 m air temperature, and precipitation. The ERA5 shows improvements over ERA-Interim in the Arctic (Hersbach *et al* 2020), due to a reduction in background errors and differences in data quality control. The ERA5 temperature and precipitation have been shown to perform well in the eastern Arctic (Graham *et al* 2019) and Alaska (White *et al* 2020). Note that summer ground-surface temperatures are usually warmer than 2 m air temperature due to the absorption of solar radiation by the land surface (Raynolds *et al* 2008). SWI is calculated as the sum of average April to September monthly surface temperatures above freezing at each pixel, in units of °C months. SWI based on the AVHRR land-surface temperatures is identified as SWIs, and SWI based on 2 m ERA5 air temperature is called SWIa. The CI is the difference between the maximum monthly air temperature and the minimum monthly air temperature for each pixel in a calendar year, in units of °C using ERA5. There are various ways to calculate the CI (Vilček *et al* 2016), but we chose the simple index, which has been used successfully at high latitudes to compare the sensitivities of mass balance in maritime and continental glaciers (De Woul and

Hock 2005). Summer precipitation (mm) is the sum over June, July and August for each pixel for each year. Finally, the AO and AD indices were calculated for winter (December–February) and summer (June–August) over the 1979–2019 period by applying empirical orthogonal analysis (Kutzbach 1967) on the seasonal ERA5 sea level pressure.

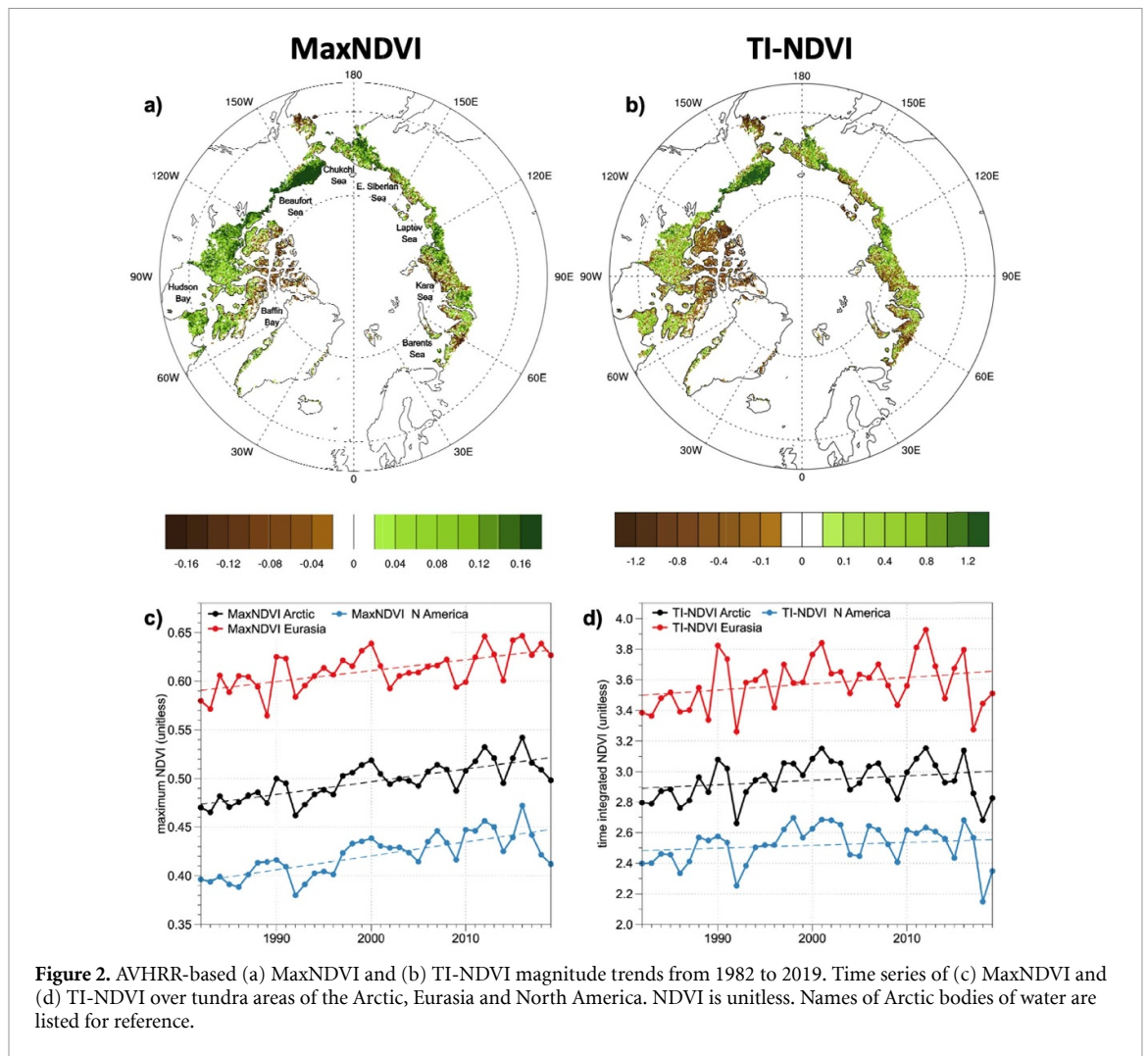
2.2. Analysis methods

Our study area was the Arctic non-alpine tundra region as defined in the Circumpolar Arctic Vegetation Map, with the southern boundary defined as treeline (CAVM Team 2003). Linear trends were calculated for time series averaged over oceanic regions within 100 km of the Arctic coastline and over the full tundra domains at elevations <300 m. Results are presented for the full Arctic, and divided into North America and Eurasia. Spatial trends in indicators are shown as maps of magnitude change over the 1982–2019 period, and the least-squares-fit method was used to determine the trends. Standard Pearson correlation coefficients and regression coefficients were calculated after all series were linearly detrended. The statistical significance of correlations and trends were assessed using the two-tailed Student's *t*-test with a 95% and 90% threshold for significance. Reduced degrees of freedom for trend significance followed Santer *et al* (2000).

3. Results

3.1. Normalized difference vegetation index

The tundra MaxNDVI and TI-NDVI trends display increases over most of the Arctic but there are also regions with declines: southwestern Alaska, high Canadian Arctic, and scattered areas of western Eurasia (figures 2(a) and (b)). There are more pixels with negative trends for TI-NDVI than for MaxNDVI over the 1982–2019 period. MaxNDVI pixels with trends lower than -0.1 account for 7% of the total in both Eurasia and North America. In contrast, TI-NDVI pixels with trends below -0.4 account for 15% of the total in Eurasia and 23% in North America. The North Slope of Alaska is the region of the Arctic with the most homogenous positive trends in MaxNDVI and TI-NDVI trends over the 1982–2019 period (figures 2(a) and (b)). Arctic MaxNDVI and TI-NDVI time series display a steady increasing trend over the 1982–2019 period though TI-NDVI shows recent declines (figures 2(c) and (d)). TI-NDVI displays a declining trajectory over the last decade that results from recent record lows: the second-lowest value was in 2017 in Eurasia and the lowest value was in 2018 in North America. The standard deviation for MaxNDVI is similar for Eurasia and North America while that for TI-NDVI is slightly higher in Eurasia (0.16) than North America (0.13) (table 1, bottom). MaxNDVI and TI-NDVI are more strongly correlated



to each other in North America (0.81) than Eurasia (0.59) (table 2).

It is generally agreed that, to the first-order, Arctic tundra plants are temperature limited (Bliss and Petersen 1992), but there is growing evidence that precipitation should also be considered in this context (e.g. Keuper *et al* 2012, van der Kolk *et al* 2016). In some regions of the Arctic, SWI trends are increasing (section 3.2) yet the corresponding NDVI trends are decreasing, suggesting additional drivers are in play. This motivates analysis of other potential climate factors, such as continentality and precipitation.

3.2. Spring SI and OW

Spring SI and summer OW both display their largest trends (decreasing for SI and increasing for OW) in the Beaufort, Chukchi, Laptev, and Kara/Barents Seas (figures 3(a) and (b)). Spring SI trends are increasing in the southern portions of the Bering Sea where North Pacific decadal variability resulted in above normal SI from 2006 to 2013 (Frey *et al* 2015). Spring SI has decreased and OW has increased over northern Baffin Bay along the northwest Greenland coast. The expansion of the ice edge poleward is greater in the western Arctic (Beaufort and Chukchi Seas)

than in the Atlantic sector (Barents and Kara Seas) (figure 3(b)), based on comparing spring SI versus summer OW trends (figures 3(a) and (b)). However, the OW trends are largest in the Atlantic sector. The SI declines and OW increases are larger on the western side of Hudson Bay compared to its eastern. OW has decreased in northeast Greenland where ice is being transported out of the Arctic Basin.

Spring SI time series for a 100 km coastal zone in the Arctic, Eurasia, and North America indicate a decline from around 60% ice cover in the early 1980s to between 30% and 40% in recent years (figure 3(c)). The SI linear trend is -18.7% , -24.0% , and -17.6% for the Arctic, Eurasia, and North America, respectively (table 1, top). Spring SI in the 100 km coastal zone has leveled off for North America in the last decade but has continued to decline in Eurasia. OW time series in the 100 km coastal zone display an increase from 40%–47% in the early 1980s to 60%–65% in recent years (figure 3(d)). The OW trend is 16.0%, 20.9%, and 13.0% for the Arctic, Eurasia, and North America, respectively (table 1). SI and OW trends and interannual variability are larger in Eurasia than North America because of the perennial SI in the high Canadian Arctic.

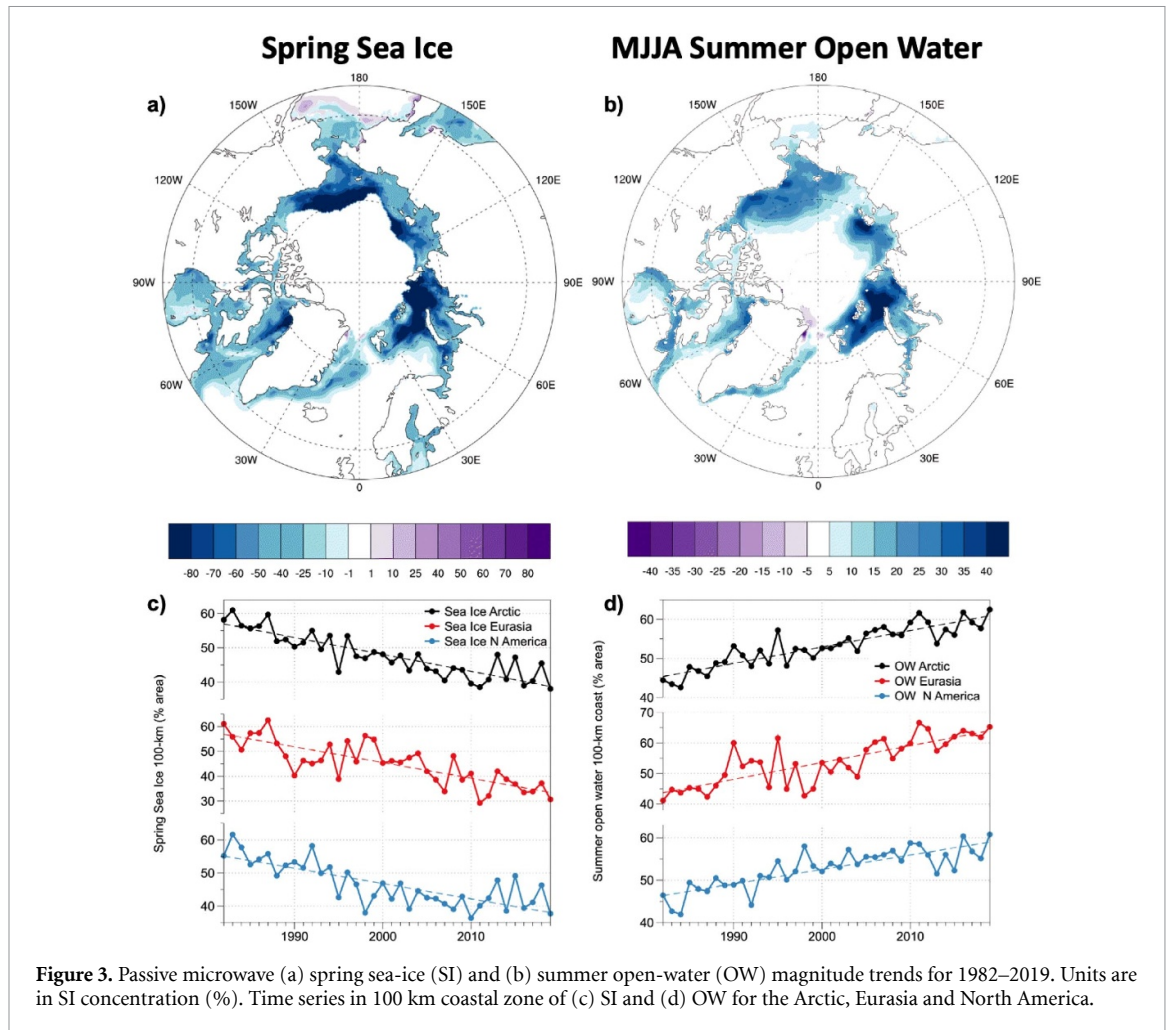
Table 1. Trends, means and standard deviations are shown for time series of sea-ice (SI), open-water (OW), summer warmth index for surface temperature (SWIs), and 2 m air temperature (SWIa), maximum (MaxNDVI) and time integrated (TI-NDVI) NDVI, continentality index (CI), and total summer precipitation (TSP). Magnitude trends are over the 38 year period from 1982 to 2019. bold (italic) indicates statistical significance at the 95% (90%) or greater level based on a *t*-test with reduced degrees of based on Santer et al (2000). Index means are shown in the middle section of the table and standard deviations are shown at the bottom.

		SI (%)	OW (%)	SWIs (°C month)	SWIa (°C month)	MaxNDVI (unitless)	TI-NDVI (unitless)	CI (°C)	TSP (cm)
Trend per 38 years	Arctic	-18.72	16.00	6.35	7.64	0.050	0.11	-1.84	0.63
	Eurasia	-24.05	20.90	4.42	8.17	0.043	0.16	-1.30	0.40
	N. America	-17.58	12.97	7.43	6.42	0.054	0.07	-3.07	1.15
Mean	Arctic	47.80	53.10	27.80	24.60	0.50	2.90	39.10	11.50
	Eurasia	45.20	53.90	30.70	23.50	0.61	3.60	40.30	11.70
	N. America	46.60	52.70	26.20	27.00	0.42	2.50	36.40	11.10
Stdev	Arctic	6.22	5.17	3.25	3.19	0.02	0.13	1.66	1.19
	Eurasia	8.66	7.52	3.71	3.75	0.02	0.16	2.12	1.58
	N. America	6.53	4.56	3.67	2.72	0.02	0.13	1.97	1.24

Table 2. Correlations for Arctic (top row each set), Eurasia (middle row) and North America (bottom row) among the key indicators within the same region. Time series were linearly detrended before correlations were calculated. Bold (italic + underlined) indicates statistical significance at the 95% (90%) or greater level based on a *t*-test.

	OW	SWIs	SWIa	MaxNDVI	TI-NDVI	CI	TSP	DJF-AD	JJA-AD
SI	-0.86	-0.11	-0.39	-0.21	-0.54	0.10	-0.11	0.11	<u>-0.29</u>
	-0.93	<u>-0.27</u>	-0.53	-0.07	-0.33	0.15	-0.22	0.37	-0.27
	-0.91	-0.15	-0.413	-0.33	-0.57	0.06	-0.35	-0.12	-0.13
OW		0.16	0.56	0.16	0.42	-0.12	0.13	-0.11	<u>0.27</u>
	1	0.21	0.55	0.08	<u>0.31</u>	-0.13	0.24	-0.29	0.33
		0.26	0.56	<u>0.29</u>	0.48	-0.12	0.45	0.16	0.05
SWIs			0.52	0.18	0.23	0.15	-0.18	0.03	-0.15
			0.74	0.34	0.36	0.14	<u>-0.29</u>	-0.11	-0.2
		1	0.62	0.14	<u>0.29</u>	0.17	0.22	0.11	-0.07
SWIa				0.23	<u>0.30</u>	0.15	-0.13	0.08	0.04
				0.17	0.43	0.13	-0.12	-0.14	0.07
				<u>0.29</u>	0.40	0.26	0.20	0.17	-0.09
MaxNDVI			1		0.76	<u>0.31</u>	0.20	-0.28	0.14
					0.59	0.09	0.11	-0.37	-0.05
				1	0.81	0.25	0.06	-0.13	0.24
TI-NDVI						<u>0.30</u>	0.17	-0.19	0.12
						0.20	0.19	<u>-0.31</u>	0.08
					1	0.19	0.10	-0.05	0.14
CI							-0.08	0.19	-0.26
							-0.23	<u>0.3</u>	-0.18
						1	0.13	-0.26	<u>-0.27</u>
								<u>-0.32</u>	0.4
TSP								-0.4	0.46
							1	0.18	-0.09

Correlation table key
 Arctic—Top
 Eurasia—Middle
 N. America—Bottom



3.3. Summer warmth index

Climatological SWI of surface temperature (SWIs) and 2 m air temperature (SWIa) (figures 4(a) and (d)) display similar overall patterns where terrestrial Arctic SWI is greater than that over the Arctic Ocean. SWIs trends for the polar region north of 55° N are largest over the ocean areas adjacent to the Arctic land areas and display a band of decreasing trends between 60° and 70° N over Siberia and in the vicinity of the Mackenzie River (figure 4(b)). SWIa trends are increasing over most of the study region and display weak trends over the Arctic SI (figure 4(e)). Since the focus of this study is Arctic tundra, subsequent discussion will focus on tundra areas shown in figures 4(c) and (f) for SWI trends though plots will show pan-Arctic values to facilitate the climate driver discussion. Regional linear trends in Eurasia are larger for SWIa than SWIs while trends in North America are larger for SWIs than SWIa (table 1, top). SWIs displays the largest increasing trends around Greenland, Baffin Island, and southwestern Alaska (figure 4(c)). SWIa has large increasing trends along the coasts of the Laptev Sea, Chukotka and southern Canadian archipelago (figure 4(f)).

SWIs and SWIa time series display increasing trends in the Arctic, Eurasia and North America

(figures 4(g) and (h)). In Eurasia, mean tundra SWIs is 30.7°C month and SWIa is 23.5°C month, about a 7°C month difference between the surface and 2 m temperatures. In contrast, in North America mean tundra SWIs and SWIa are 26.2°C and 27°C month, respectively (table 1, center). It is noteworthy that the SWIs mean is lower than the SWIa, in disagreement with previous comparisons (e.g. Bhatt *et al* 2017). The large 2 m air temperature-based SWI in North America arise from mean ERA5 SWIa over western Alaska tundra regions that are larger than mean SWIs in the same region (figures 4(a) and (d)). These SWI values if correct suggest large poleward heat transport in the Pacific sector but may also arise erroneously and warrant further investigation in the ERA5, which is beyond the scope of the current study. The interannual variability quantified by the standard deviation is slightly higher in Eurasia than for North America for both SWIs and SWIa (table 1, bottom). The SWIs over Eurasia and N. America decreased from 2000 to 2010, suggesting low-frequency climate variations present during the summer over Arctic tundra.

3.4. Continentality index

The Arctic tundra is a maritime biome (Walker *et al* 2005), and the trend in the CI ($T_{\text{max}} - T_{\text{min}}$ of average

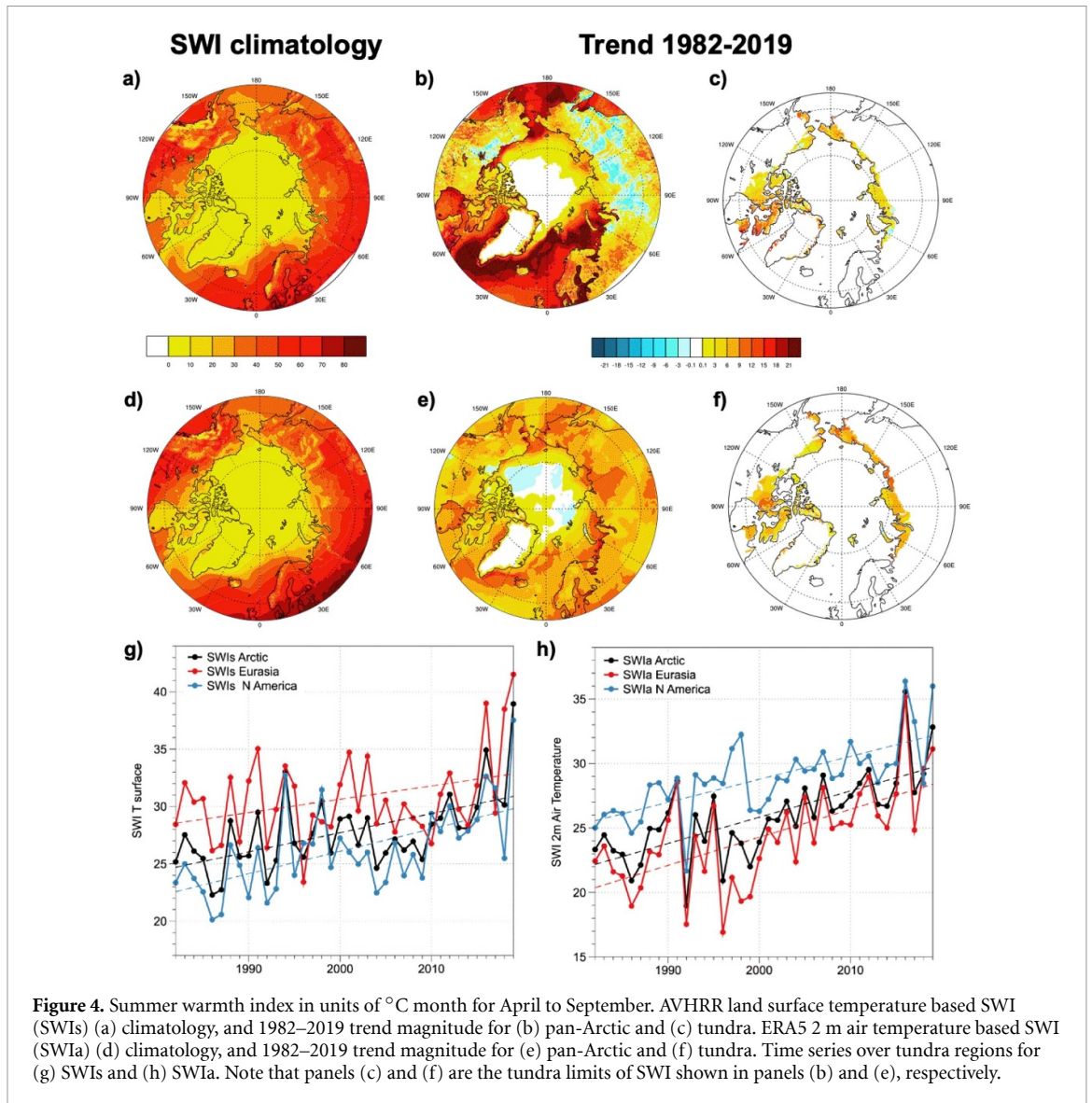


Figure 4. Summer warmth index in units of °C month for April to September. AVHRR land surface temperature based SWI (SWIs) (a) climatology, and 1982–2019 trend magnitude for (b) pan-Arctic and (c) tundra. ERA5 2 m air temperature based SWI (SWIa) (d) climatology, and 1982–2019 trend magnitude for (e) pan-Arctic and (f) tundra. Time series over tundra regions for (g) SWIs and (h) SWIa. Note that panels (c) and (f) are the tundra limits of SWI shown in panels (b) and (e), respectively.

monthly temperatures in a calendar year) reflects the increasing maritime influence caused by more near-shore OW. The climatological CI is characterized by small values (0 °C–20 °C) over the ocean and larger values (40 °C–65 °C) over land (figure 5(a)). The climatological CI is the largest over Eastern Siberia where winters are extremely cold and summers are warm. The western portions of Eurasia and North America have a lower mean CI than regions farther east, consistent with the strength of maritime influence in generally eastward atmospheric flow. Regarding tundra, eastern Eurasia and the Canadian Arctic have the largest CI values. The CI has decreased over most of North America and has mixed trends over Eurasia (figure 5(b)). Trends over tundra regions are generally decreasing.

Time series of the CI display decreasing trends over Eurasian and North American tundra regions (figure 5(c)). The CI trend over North America is -3.07 °C/38 years (significant at the 95% or greater level) and over Eurasia is -1.83 °C/38 years (table 1,

top). North American tundra has become more maritime over the 1982–2019 period than has Eurasian tundra. The mean CI index over tundra is larger for Eurasia than North America (table 1, middle) and the CI index standard deviation is slightly higher for Eurasia than North America (table 1, bottom).

3.5. Precipitation

Quantifying precipitation with confidence in the Arctic remains a challenge but it is an important indicator for vegetation and will increase in importance as the climate warms. This study employs precipitation from ERA5, which appears to be a substantial improvement over previous products in the Arctic and less prone to discontinuities in Alaska compared to station observations (White *et al* 2020). The June–August (TSP) ranges between 5 and 20 cm over the tundra (figure 6(a)). Mean precipitation is higher on the western versus the eastern sides of Eurasia and North America, which is consistent with the

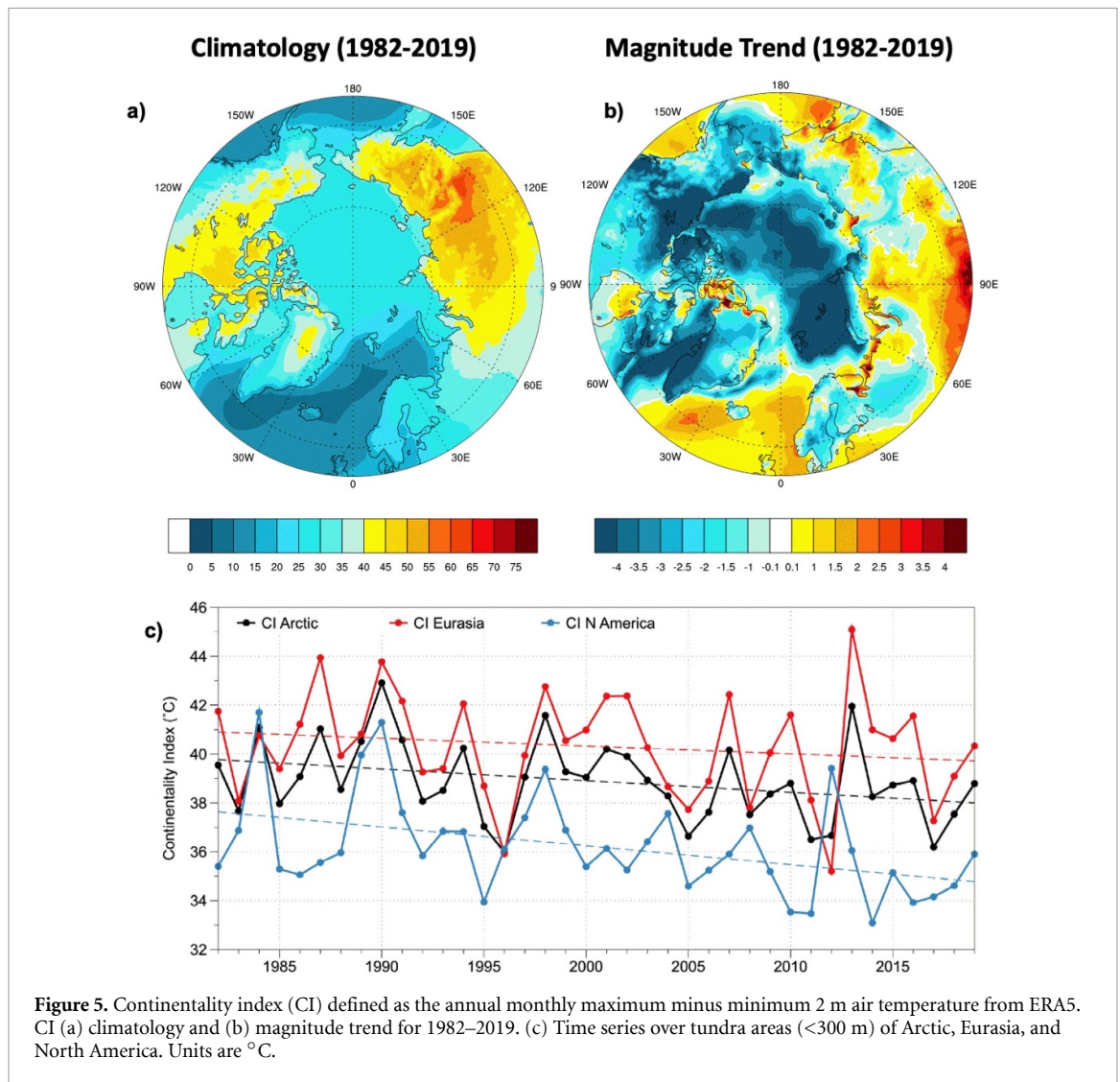


Figure 5. Continuity index (CI) defined as the annual monthly maximum minus minimum 2 m air temperature from ERA5. CI (a) climatology and (b) magnitude trend for 1982–2019. (c) Time series over tundra areas (<300 m) of Arctic, Eurasia, and North America. Units are °C.

mean continuity gradient (figure 5(a)). Climatological precipitation is higher in those parts of the Arctic at higher elevations. Trends in precipitation over the 1982–2019 period display areas of increasing and decreasing trends in the Arctic but are generally increasing over the tundra regions, particularly in North America (figure 6(b)). The trend in tundra precipitation over North America is 1.15 cm/38 years (significant at the 90% or greater level) (table 1). The trend over Eurasian tundra is weak and not significant (0.40 cm/38 years). Similar to other indicators, the standard deviation in Eurasia is higher than North America for TSP, 1.58 versus 1.24 cm (table 1).

3.6. AO and AD index

The discussion of indicators in the Arctic would be incomplete if indices describing variability of atmospheric circulation, such as the AO and the AD, were not explored. These teleconnection indices can provide insight into the large-scale atmospheric drivers (e.g. Macias-Fauria *et al* 2012) that force SI which then influences tundra vegetation. Both indices are linear decompositions of sea level pressure using

empirical orthogonal functions (EOF) or principal component analysis (PCA). This method separates differ parts of a signal into a few patterns that maximize variability and is similar to ordination of vegetation using PCA (Anderson 1971). The AO (Thomson and Wallace 1998) is the first EOF of atmospheric sea level pressure and the variance explained is 31.6% in DJF and 30.5% in JJA. The AD is the second EOF and the variance explained is 13.8% in DJF and 12.3% in JJA, less than half that of the AO. The AO is correlated with many physical and biological metrics in the Arctic (e.g. Baltzer *et al* 2005, Rigor *et al* 2002) but was weakly correlated with tundra indicators in both seasons, so we only present the AD results. The AD (Wu *et al* 2006) explains less variance than the AO but is important for SI variations and particularly the transpolar movement of SI exiting the Arctic which coincides with the transition zone between the anomalous high and low (figures 7(a) and (b)). Note that in the northern hemisphere low pressure has counter-clockwise circulation while high pressure has clockwise circulation. The time series in figure 7(c) represents how the patterns vary over time. The magnitude

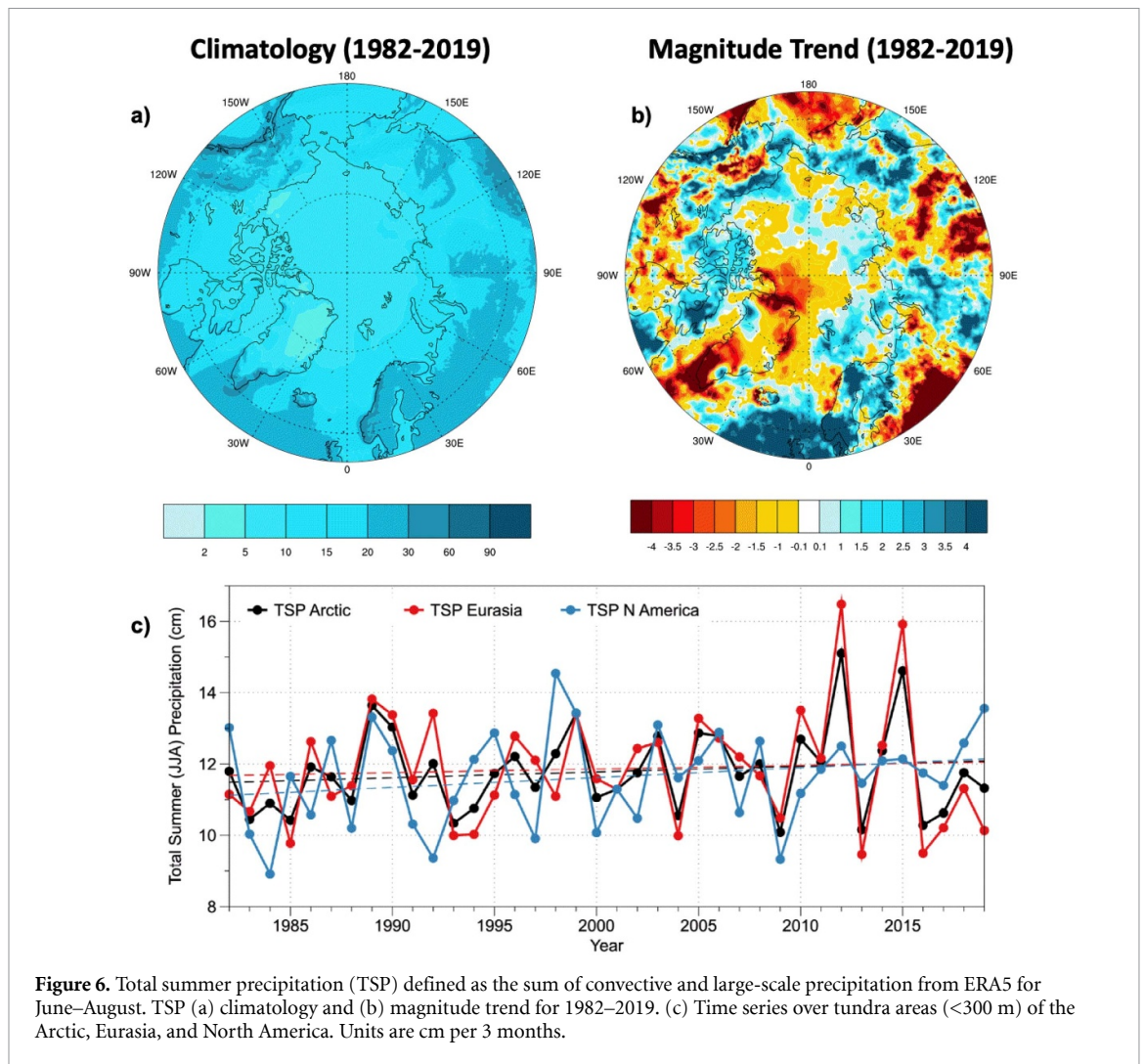


Figure 6. Total summer precipitation (TSP) defined as the sum of convective and large-scale precipitation from ERA5 for June–August. TSP (a) climatology and (b) magnitude trend for 1982–2019. (c) Time series over tundra areas (<300 m) of the Arctic, Eurasia, and North America. Units are cm per 3 months.

trend over the 38 years of the study period is -0.58 for DJF-AD and 0.95 JJA-AD. Cai *et al* (2018) showed that the AD is linked to observed temperature and precipitation variations using the ERA-Interim and evaluated these relationships in a suite of CMIP5 models. One key finding of Cai *et al* (2018) was that the AD had a larger impact on precipitation variations than on temperature. The DJF-AD and the JJA-AD were significantly correlated with some of the tundra indicators and this is explored further in the discussion of covariability of indices.

4. Discussion of covariability among indicators

Based on linearly detrended correlations between the indicators, we find that SI continues to influence tundra vegetation. Above average spring SI corresponds to below average OW, SWIa and TI-NDVI (table 2), consistent with previous studies (e.g. Dutrieux *et al* 2012, Bhatt *et al* 2017). However, the influence of SI on tundra indicators is not as strong as it was before based on a comparison of correlations over

1982–2019 to 1982–2008 (table 3). In Eurasia, correlations between SI have weakened with SWIs and TI-NDVI (table 3). In North America, correlations are weaker between SI and SWIs but have increased slightly with TI-NDVI (table 3). Additionally, the correlation between SWIs and TI-NDVI has weakened substantially in both Eurasia and North America (table 3). This suggests a weakening influence of SI and land surface temperatures on tundra vegetation productively and the emergence of other forcing factors over the last decade. Atmospheric moisture is a likely factor that may be gaining importance in the tundra story. In North America, significant correlations demonstrate that anomalously high OW results in above normal MaxNDVI and greater precipitation. TSP is weakly correlated in Eurasia and North America with the other indicators, leading us to conclude that moisture as a climate driver for tundra variability has not yet emerged but will as tundra regions become more maritime as the OW increases and the CI decreases.

The CI index was significantly correlated with only Arctic MaxNDVI and TI-NDVI (table 2) at 0.31 and 0.30, respectively (significant at the 90%

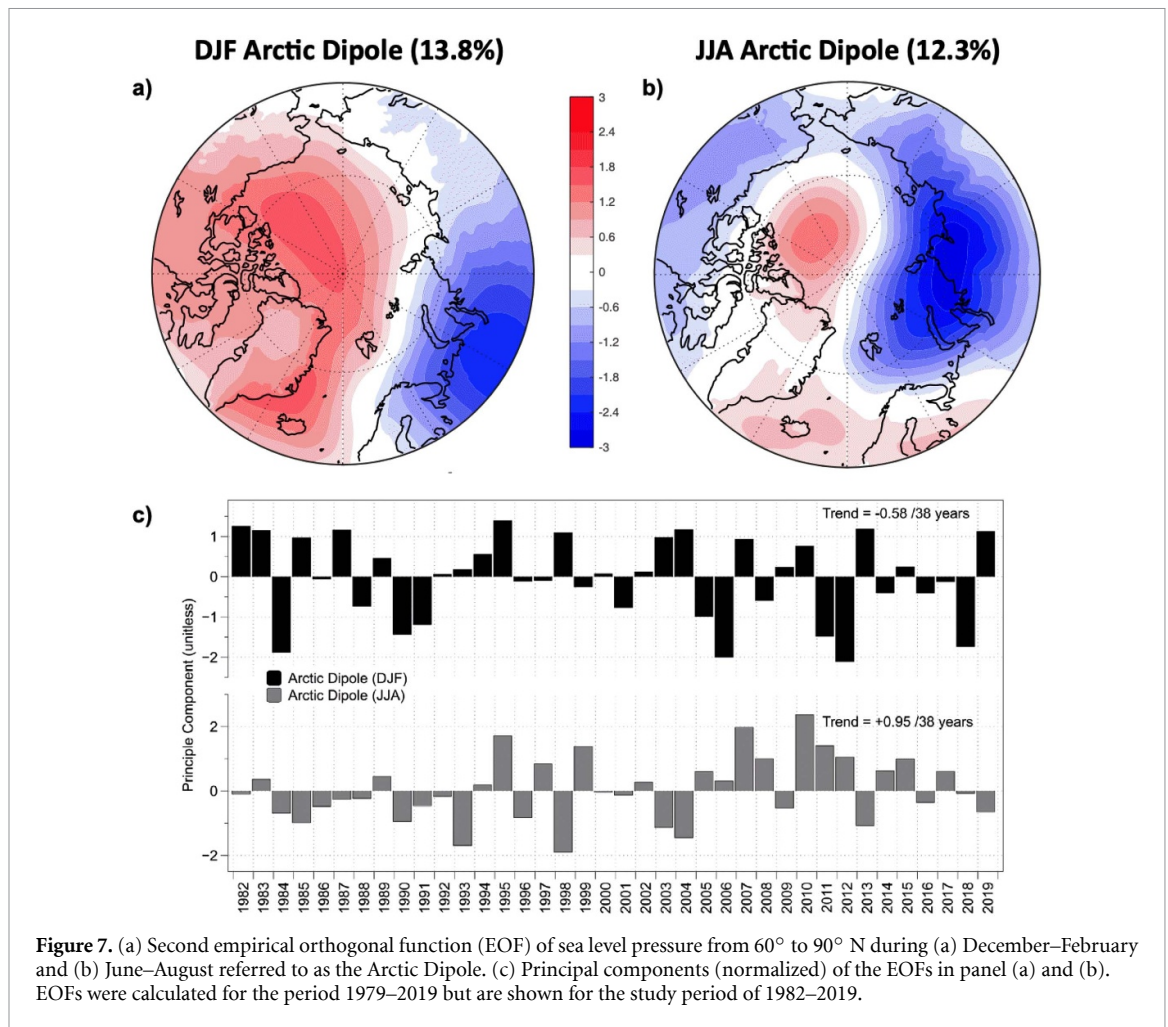


Figure 7. (a) Second empirical orthogonal function (EOF) of sea level pressure from 60° to 90° N during (a) December–February and (b) June–August referred to as the Arctic Dipole. (c) Principal components (normalized) of the EOFs in panel (a) and (b). EOFs were calculated for the period 1979–2019 but are shown for the study period of 1982–2019.

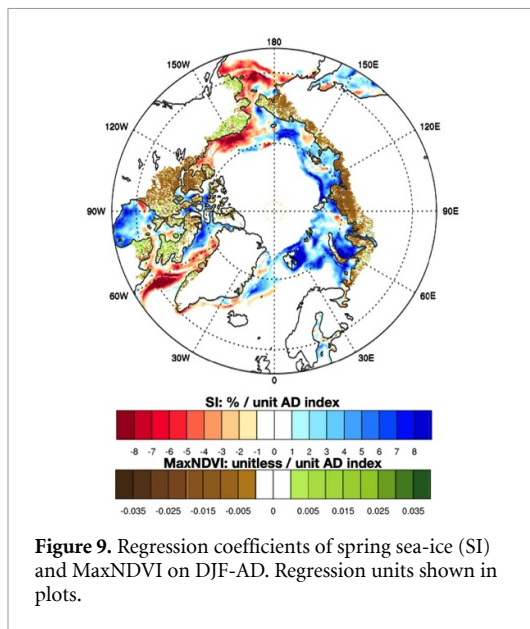
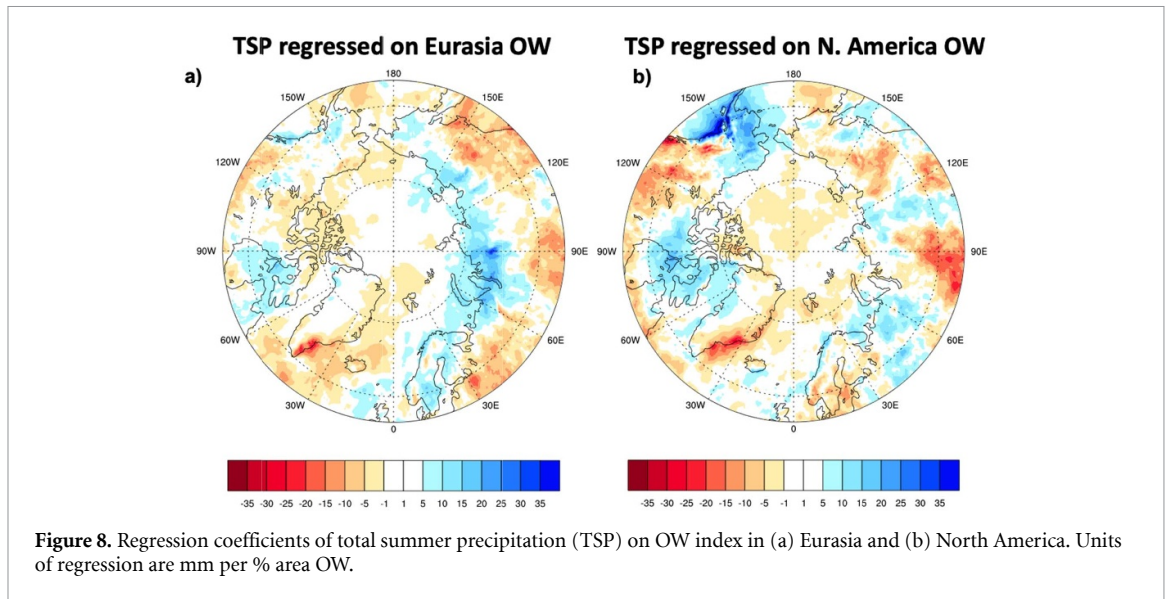
Table 3. Select correlations from table 2 for 1982–2019 compared to 1982–2008 from Bhatt *et al* (2010). © American Meteorological Society. Used with permission. Time series were linearly detrended before correlations were calculated. Bold (italic + underlined) indicates statistical significance at the 95% (90%) or greater level based on a t-test.

	Correlation with Sea Ice				Correlation with SWIs	
	SWIs 82-19	SWIs 82-08	TI-NDVI 82-19	TI-NDVI 82-08	TI-NDVI 82-19	TI-NDVI 82-08
Arctic	-0.11	-0.49	-0.54	-0.56	0.23	0.64
Eurasia	<u>-0.27</u>	-0.58	-0.33	-0.51	0.36	0.67
N. America	-0.15	-0.56	-0.57	-0.53	<u>0.29</u>	0.60

or greater level). Correlations between the Arctic CI index and spatial TI-NDVI are increasing throughout most of the tundra region though weak (<0.3, not shown). The stronger correlation at the pan-Arctic scale than the continental scale highlights the notion that key driving processes vary with region and scale, which adds challenges to identifying drivers (Myers-Smith *et al* 2020). The CI does not seem to contribute substantially at present to tundra vegetation productivity variability. However, a continued decrease of continentality driven by SI decline could make CI a more important climate driver in the future (table 1).

TSP is significantly correlated with SWIs (-0.29, ≥90%) in Eurasia and SI (-0.35, ≥95%) and OW (0.45, ≥95%) in North America (table 2). This

suggests that above normal precipitation corresponds to reduced SI and enhanced OW in North America. This interpretation is confirmed by regression coefficients of TSP on Eurasian and North American OW (figures 8(a) and (b)), where positive precipitation anomalies correspond to above normal OW in their respective regions. While the correlations of indicators are very weak, precipitation is positively correlated with Max-NDVI and TI-NDVI for the Arctic, Eurasia and North America, where the correlations are somewhat stronger in Eurasia than North America. We speculate that the importance of precipitation as a climate driver for tundra NDVI may increase in the future as the climate warms, evapotranspiration increases, and permafrost thaw alters near-surface soil hydrology.

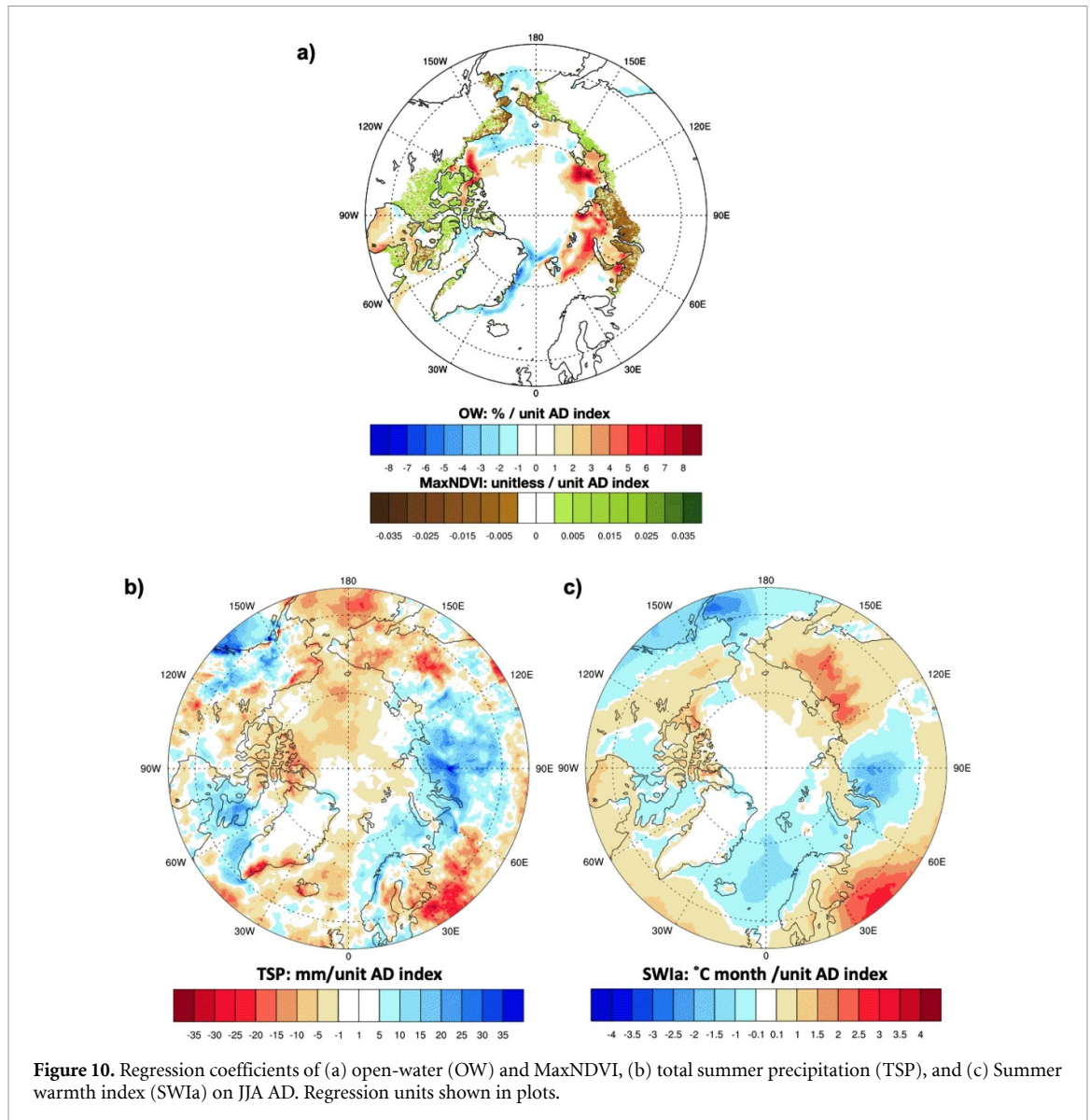


A new finding of this study is that SI and OW are more strongly correlated with SWIa than SWIs in all of the regions (table 2), where above normal SI corresponds to below normal SWIa and SWIs. Although the datasets underlying the two SWI indicators come from very different sources, the much weaker correlations of SWIs relative to SWIa suggest that the strong influence of vegetation and seasonal snow on the Arctic surface energy budget has dampened this relationship between SWIs and the other indicators from previous analyses.

The DJF-AD was significantly ($\geq 90\%$) correlated with SI, OW, MaxNDVI, TI-NDVI, CI, and TSP, while the JJA-AD was correlated with OW and TSP. This appears surprising at first but is consistent with the following sequence: the DJF-AD forces spring SI anomalies that then drive summer temperature, precipitation, and tundra NDVI variations. Correlations

(table 2) indicate that the positive phase of the DJF-AD is associated with greater spring SI in the Eurasian 100 km coastal zone, reduced summer OW, below average Max and TI-NDVI, and below normal precipitation. Regressions provide a spatial perspective: positive DJF-AD departures are associated in Eurasia with positive SI and negative MaxNDVI anomalies and in the Alaska seas with negative SI and positive MaxNDVI anomalies (figure 9(a)). The DJF AD drives SI variations which then force SWIa and NDVI anomalies in the following summer. The DJF AD connection with summer NDVI motivates examining precipitation in preceding seasons in the future as another potential climate driver. The two-season lag relationships provide the basis for multiseasonal predictions for which skill measures (i.e. how well a forecast performs) will exceed those of random chance and of climatology.

The positive phase of the JJA-AD enhances offshore flow over Eurasia (figure 7(b)) to increase OW, which is consistent with the significant positive correlations between JJA-AD and OW (table 2). This is confirmed from the spatial perspective with regressions of OW on JJA-AD (figure 10(a)). Correlations of MaxNDVI and JJA-AD are weak but when regressed on JJA-AD (figure 10(a)) the patterns reveal a varied structure over Eurasia. Eurasia west of 120° E shows that more OW is associated with MaxNDVI declines, which appears inconsistent with positive correlations between NDVI and OW found in table 2. This is explored further by constructing regressions of SWI and TSP on JJA-AD. A consistent explanation emerges when all the variables are examined in the context of the JJA-AD in western Eurasia: the above normal OW and negative MaxNDVI anomalies correspond to positive precipitation (figure 10(b)) and negative temperature (figure 10(c)) departures. In the Laptev Sea the regression on JJA-AD indicates that enhanced OW corresponds to positive MaxNDVI



anomalies (figure 10(a)), above normal precipitation (figure 10(b)), and above normal SWIa (figure 10(c)). OW has a spatially varied but consistent covariability in Eurasia with adjacent SWIa, MaxNDVI, and TSP. This result highlights the value of indicators at the large-scale and the need for caution when trying to generalize relationships regionally. In particular, the spatial pattern of the JJA-AD is such that offshore flow, above-normal temperatures and reduced SI are favored under the positive JJA-AD in eastern Eurasia (Laptev, East Siberian Seas), while onshore flow and colder-than-normal temperatures are favored over eastern Eurasia (Barents, Kara Seas).

5. Summary and conclusions

In this study, climate indicators known to be relevant for tundra productivity (i.e. coastal SI, coastal summer OW, SWI), two additional indicators (continentality and summer precipitation), and Arctic teleconnection indices (AO and AD) are analyzed for

trends and co-variability in the context of Max and TI-NDVI. Over the study period of 1982–2019, significant decreasing trends in spring SI and significant increasing trends in summer OW, SWI (SWIs, SWIa) and MaxNDVI present a consistent story over Eurasia and North America. Despite a decline in recent years, TI-NDVI still displays overall increasing trends, though they are only statistically significant in Eurasia. Spatial TI-NDVI trends show declines in the Canadian High Arctic and southwest Alaska. High Arctic TI-NDVI declines may be due to thawing permafrost, melting ground ice and subsidence arising from high sensitivity to increasing SWIs because vegetation is sparse and organic layers are thin (Farquharson *et al* 2019). The CI has decreasing trends over tundra in Eurasia and North America, with significance ($\geq 95\%$) only for the latter. CI's relevance for tundra may increase since it is expected to continue to decrease in the future as warming is projected to be greater in winter than summer. TSP is increasing over Eurasia and North America,

with the latter having weakly significant trends ($\geq 90\%$).

Correlation analysis identifies large-scale covariability between the indicators. The most significant correlations are between TI-NDVI and the climate indicator variables: above normal TI-NDVI corresponds to below normal SI (a spring indicator), and above normal OW, SWIs, and SWIa. TI-NDVI better reflects total seasonal productivity rather than peak biomass and is also a better tool for exploring changes in the growing season associated with more OW and changes in the timing of greenup and senescence. Correlations between SI and summer warmth and TI-NDVI have weakened when analyzed over the 1982–2019 period compared to 1982–2008 (Bhatt *et al* 2010) suggesting other processes are operating to change the influence of SI on tundra vegetation. The atmospheric mode of variability named the AD is defined as the second EOF of sea level pressure and was more closely correlated to the tundra indicators than the AO. In particular, winter AD is significantly correlated in Eurasia with SI, OW, MaxNDVI, TI-NDVI, CI and TSP. At first a winter connection to tundra productivity is perplexing but the link is through SI. The DJF-AD drives SI variations which shape OW, SWIa and NDVI anomalies during the following summer. This connection with DJF-AD has potential for use in prediction of Arctic vegetation variability.

Spatial regressions on JJA-AD demonstrate how the large-scale circulation favors regional climate anomalies that have competing effects on tundra vegetation. Above normal OW in the Kara–Barents Seas is associated with below normal MaxNDVI on adjacent land, above normal summer precipitation, and below normal SWIa during the positive phase of the JJA-AD. In contrast, in the Laptev Sea, above normal OW is associated with above normal MaxNDVI, TSP, and SWIa during the positive phase of the JJA-AD. This hints at potential competing effects of OW on TSP and SWIa and supports examining the climate drivers of tundra vegetation further at the regional scale.

It is challenging to synthesize climate driver understanding across scales: from plot to landscape to region to continent to hemisphere. The importance of a given climate driver likely varies with scale, and further work to understand across-scale relationships (e.g. Assmann *et al* 2020) is needed. Regional scale studies using the indicators framework may be fruitful, and the inclusion of other parameters such as cloud and snow cover would be an important next step. Clouds and snow cover are likely changing in the Arctic and both are relevant for tundra vegetation productivity. Clouds, precipitation, and surface snow cover are among the most challenging parameters for earth system models (Kushner *et al* 2018, McIlhatten *et al* 2020) to simulate, let alone

predict, yet these are key for vegetation productivity. Advancing our understanding of climate drivers of tundra vegetation is relevant for Arctic prediction on seasonal-to-decadal scales and needed to anticipate future water and carbon budgets. While the indicator framework presented in this study shows the potential for seasonal prediction, climate model simulations will be required to quantify the likelihood of future changes in Arctic vegetation over decadal and longer timescales.

Data availability statement

The data that support the findings of this study are available upon reasonable request from the authors.

Acknowledgments

This work was supported by the Climate Program Office of the National Oceanic and Atmospheric Administration through Grant No. NA17OAR4310160. USB, GJF, and ASH acknowledge support from NASA NNH16CP09C grant as part of the Arctic Boreal Vulnerability Experiment. DAW and MKR acknowledge support from Award Number 1263854 from the National Science Foundation.

ORCID iDs

Uma S Bhatt  <https://orcid.org/0000-0003-1056-3686>

Josefino C Comiso  <https://orcid.org/0000-0002-0875-7433>

Gerald V Frost  <https://orcid.org/0000-0002-5134-0334>

References

- Anderson A J B 1971 Ordination methods in ecology *J. Ecol.* **59** 713–26
- Assmann J J, Myers-Smith I H, Kerby J T, Cunliffe A M and Daskalova G N 2020 Drone data reveal heterogeneity in tundra greenness and phenology not captured by satellites *Environ. Res. Lett.* **15** 125002
- Balzer H *et al* 2005 Impact of the Arctic Oscillation pattern on interannual forest fire variability in Central Siberia *Geophys. Res. Lett.* **32**
- Bhatt U S *et al* 2010 Circumpolar Arctic tundra vegetation change is linked to sea-ice decline *Earth Interact.* **14** 1–20
- Bhatt U S *et al* 2017 Changing seasonality of panarctic tundra vegetation in relationship to climatic variables *Environ. Res. Lett.* **12**
- Bhatt U S, Walker D A, Reynolds M K, Bieniek P A, Epstein H E, Comiso J C, Pinzon J E, Tucker C J and Polyakov I V 2013 Recent declines in warming and Arctic vegetation greening trends over pan-Arctic tundra *Remote Sens.* **5**
- Bintanja R and Selten F M 2014 Future increases in Arctic precipitation linked to local evaporation and sea-ice retreat *Nature* **509** 479–82
- Bjerke J W, Treharne R, Vikhamar-Schuler D, Karlsen S R, Ravolaine V, Bokhorst S F, Phoenix G K, Bochenek Z and

- Tommervik H 2017 Understanding the drivers of extensive plant damage in boreal and Arctic ecosystems: insights from field surveys in the aftermath of damage *Sci. Total Environ.* **599–600** 1965–76
- Bliss L C and Peterson K M 1992 Plant succession, competition, and the physiological constraints of species in the Arctic *In Arctic Ecosystems in a Changing Climate* (New York: Academic) pp 111–36
- Bokhorst S F, Bjerke J W, Tommervik H, Callaghan T V and Phoenix G K 2009 Winter warming events damage sub-Arctic vegetation: consistent evidence from an experimental manipulation and a natural event *J. Ecol.* **97** 1408–15
- Box J E *et al* 2019 Key indicators of Arctic climate change: 1971–2017 *Environ. Res. Lett.* **14** 045010
- Cai L, Alexeev V A, Walsh J E and Bhatt U S 2018 Patterns, impacts, and future projections of summer variability in the Arctic from CMIP5 models *J. Clim.* **31**
- Campbell T K F, Lantz T C, Fraser R H and Hogan D 2020 High Arctic vegetation change mediated by hydrological conditions *Ecosystems* (<https://doi.org/10.1007/s10021-020-00506-7>)
- CAVM Team 2003 Circumpolar Arctic vegetation map (1:7,500,000 scale), conservation of Arctic Flora and Fauna (CAFF) Map No. 1. U.S. Fish and Wildlife Service (Anchorage, Alaska)
- Comiso J C 2003 Warming trends in the Arctic from clear sky satellite observations *J. Clim.* **16**
- Comiso J C and Nishio F 2008 Trends in the sea ice cover using enhanced and compatible AMSR-E, SSM/I, and SMMR data *J. Geophys. Res.* **113** C02S07
- De Woul M and Hock R 2005 Static mass-balance sensitivity of Arctic glaciers and ice caps using a degree-day approach *Ann. Glaciol.* **42** 217–24
- Dutrieux L P, Bartholomeus H, Herold M and Verbesselt J 2012 Relationships between declining summer sea ice, increasing temperatures and changing vegetation in the Siberian Arctic tundra from MODIS time series (2000–11) *Environ. Res. Lett.* **7** 044028
- Farquharson L M, Romanovsky V E, Cable W L, Walker D A, Kokelj S V and Nicolovsky D 2019 Climate change drives widespread and rapid thermokarst development in very cold permafrost in the Canadian High Arctic *Geophys. Res. Lett.* **46** 6681–9
- Frey K E, Moore G W K, Cooper L W and Grebmeier J M 2015 Divergent patterns of recent sea ice cover across the Bering, Chukchi, and Beaufort seas of the Pacific Arctic Region *Prog. Oceanogr.* **136** 32–49
- Frost G V *et al* 2020 Tundra Greenness *Arctic Report Card 2020* R L Thoman J Richter-Menge and M L Druckenmiller ed (<https://doi.org/10.25923/46rm-0w23>)
- Graham R M, Hudson S R and Maturilli M 2019 Improved performance of ERA5 in Arctic gateway relative to four global atmospheric reanalyses *Geophys. Res. Lett.* **46** 6138–47
- Hersbach H *et al* 2020 The ERA5 global reanalysis *Q. J. R. Meteorol. Soc.* **146** 1999–2049
- Jia G J, Epstein H E and Walker D A 2003 Greening of arctic Alaska, 1981–2001 *Geophys. Res. Lett.* **30**
- Kenney M A, Janetos A C and Lough G C 2016 Building an integrated US national climate indicators system *In The US National Climate Assessment* ed K Jacobs, S Moser and J Buizer (Berlin: Springer) pp 85–96
- Keuper F, Parmentier F J W, Blok D, van Bodegom P M, Dorrepaal E, van Hal J R, van Logtestijn R S P and Aerts R 2012 Tundra in the rain: differential vegetation responses to three years of experimentally doubled summer precipitation in Siberian shrub and Swedish bog tundra *Ambio* **41** 269–80
- Kushner P J *et al* 2018 Canadian snow and sea ice: assessment of snow, sea ice, and related climate processes in Canada's Earth system model and climate-prediction system *Cryosphere* **12** 1137–56
- Kutzbach J E 1967 Empirical eigenvectors of sea-level pressure, surface temperature and precipitation complexes over North America *J. Appl. Meteorol. Clim.* **6** 791–802
- Lara M J, Nitze I, Grosse G, Martin P and McGuire A D 2018 Reduced arctic tundra productivity linked with landform and climate change interactions *Sci. Rep.* **8** 2345
- Macias-Fauria M, Forbes B C, Zetterberg P and Kumpula T 2012 Eurasian Arctic greening reveals teleconnections and the potential for structurally novel ecosystems *Nat. Clim. Change* **2** 613–8
- McIlhatten E A, Kay J E and L'Ecuyer T S 2020 Arctic clouds and precipitation in the community earth system model version *J. Geophys. Res.: Atmos.* **125** e2020JD032521
- Myers-Smith I H *et al* 2020 Complexity revealed in the greening of the Arctic *Nat. Clim. Change* **10** 106–17
- Myneni R B, Keeling C D, Tucker C J, Asrar G and Nemani R R 1997 Increased plant growth in the northern high latitudes from 1981 to 1991 *Nature* **386** 698–702
- National Academies of Sciences, Engineering, and Medicine 2017 *Accomplishments of the U S Global Change Research Program* (Washington, DC: The National Academies Press) (<https://doi.org/10.17226/24670>)
- Overland J E, Wang M and Box J E 2019 An integrated index of recent pan-Arctic climate change *Environ. Res. Lett.* **14** 035006
- Pinzon J and Tucker C 2014 A non-stationary 1981–2012 AVHRR NDVI3g time series *Remote Sens.* **6** 6929–60
- Raynolds M K *et al* 2019 A raster version of the circumpolar arctic vegetation map (CAVM) *Remote Sens. Environ.* **232** 111297
- Raynolds M K and Walker D A 2016 Increased wetness confounds Landsat-derived NDVI trends in the central Alaska North Slope region 1985–2011 *Environ. Res. Lett.* **11** 085004
- Raynolds M K, Walker D A, Munger C A, Vonlanthen C M and Kade A N 2008 A map analysis of patterned-ground along a North American Arctic Transect *J. Geophys. Res.* **113** G03S03
- Richter-Menge J, Druckenmiller M L and Jeffries M ed 2019 Arctic report card 2019 (available at: www.arctic.noaa.gov/Report-Card)
- Rigor I G, Wallace J M and Colony R L 2002 Response of sea ice to the Arctic Oscillation *J. Clim.* **15** 2648–63
- Santer B D, Wigley T M L, Boyle J S, Gaffen D J, Hnilo J J, Nychka D, Parker D E and Taylor K E 2000 Statistical significance of trends and trend differences in layer-average atmospheric temperature time series *J. Geophys. Res.* **105** 7337–56
- Thompson D W and Wallace J M 1998 The Arctic Oscillation signature in the wintertime geopotential height and temperature fields *Geophys. Res. Lett.* **25** 1297–300
- Trofaiar A M, Bartsch A, Rees W G and Leibman M O 2013 Assessment of spring floods and surface water extent over the Yamalo-Nenets Autonomous District *Environ. Res. Lett.* **8** 045026
- Tucker C J 1977 Use of near infrared/red radiance ratios for estimating vegetation biomass and physiological status *NASA Technical Report X-923-77-183* pp 41 (<https://ntrs.nasa.gov/citations/19770025621>)
- Tucker C J 1979 Red and near-infrared linear combinations for monitoring vegetation *Remote Sens. Environ.* **8** 127–50
- Tucker J and Sellers P J 1986 Satellite remote sensing of primary production *Int. J. Remote Sens.* **7** 1395–416
- van der Kolk H J, Heijmans M M, van Huissteden J, Pullens J W and Berendse F 2016 Potential Arctic tundra vegetation shifts in response to changing temperature precipitation and permafrost thaw *Biogeosciences* **13** 6229–45
- Vilček J, Škvarenina J, Vido J, Nalevanková P and Kandrák R 2016 Minimal change of thermal continentality in Slovakia within the period 1961–2013 *Earth Syst. Dyn.* **7**
- Walker D A *et al* 2005 The circumpolar arctic vegetation map *J. Veg. Sci.* **16** 267–82

- Walker D A *et al* 2016 Circumpolar Arctic vegetation: a hierarchic review and roadmap toward an internationally consistent approach to survey, archive and classify tundra plot data *Environ. Res. Lett.* **11** 055005
- Wang J and Ikeda M 2000 Arctic oscillation and Arctic sea-ice oscillation *Geophys. Res. Lett.* **27** 1287–90
- White J, Walsh J E and Thoman R 2020 Using Bayesian statistics to detect trends in Alaskan precipitation *Int. J. Clim.* online accepted (<https://doi.org/10.1002/joc.6946>)
- Wu B, Wang J and Walsh J E 2006 Dipole anomaly in the Winter Arctic atmosphere and its association with sea ice motion *J. Clim.* **19** 210–25